

Nafion membranes for e-fuel cell applications

Xingyi Shi^{#,1}, Yining Ma^{#,1}, Xiaoyu Huo¹, Oladapo Christopher Esan¹, Liang An^{*,1}

¹ Department of Mechanical Engineering, The Hong Kong Polytechnic University, Hung Hom, Kowloon, Hong Kong SAR, China

[#] These authors contributed equally to this work.

^{*} Corresponding author.

Email: liang.an@polyu.edu.hk (L. An)

Abstract

Direct liquid fuel cells have been extensively studied and regarded as a promising candidate for wide commercialization among the various existing energy conversion technologies. However, their real applications still encounter many challenges mostly arising from the sluggish reaction kinetics of the liquid fuels. Recently, a novel system, powered with an electrically rechargeable liquid fuel (e-fuel), named the e-fuel cell has been presented with superior cell performance. However, studies regarding ion exchange membrane, which is an indispensable component in the liquid e-fuel cell, are still limited. Herein, a comparative study has been conducted to evaluate the performance of four Nafion series membranes. These membranes with different thicknesses have been examined and characterized at both membrane-level and cell-level. It is found that the thickness of membrane shows critical effects on its area resistance, as well as vanadium-ion crossover rate, which further significantly affects the e-fuel cell performance. Overall, the thinnest membrane (Nafion 211) is revealed to be preferable for the purpose of attaining a high peak power density, while the thickest membrane (Nafion 117) provides a lower self-discharge rate for the cell.

Keywords: E-fuel; Fuel cells, Liquid e-fuel cells; Nafion membranes; Membrane thickness;
Vanadium-ion permeability; Conductivity

1. Introduction

In the recent years, the depletion of fossil fuels as well as the increasing demand for energy across the globe have drawn widespread attention towards the development and application of renewable power sources.¹⁻⁶ As a promising energy conversion systems for sustainable power generation, fuel cells have therefore been deeply investigated since the 19th century for continuous conversion of chemical energy into electricity.^{4, 7, 8} Among the various types of fuel cell, hydrogen-oxygen fuel cells with their zero-emission feature and high-power density are regarded as a potential candidate for commercial applications.^{3, 9, 10} However, the commercialization progress of the hydrogen-oxygen fuel cells still faces some critical challenges associated with the difficulties arising from the hydrogen production, storage, and transportation.^{7, 11, 12} Alternatively, direct liquid fuel cells, which employ liquid alcohol fuels, have been extensively studied due to their higher energy density and easier fuel handling.^{2, 11, 13, 14} Nonetheless, the performance of these conventional liquid fuel cells is still greatly limited by the slow kinetics of alcohol liquid fuels oxidation reaction, which therefore requires the development of other potential liquid fuels with superior reactivity.^{11, 15, 16}

Most recently, a novel electrically rechargeable liquid fuel (e-fuel) system has been proposed and studied.^{8, 17, 18} In contrast with the conventional fuel cells and redox flow batteries, this e-fuel system possesses many advantages including almost instantaneous rechargeability. In our previous studies, an e-fuel cell fed with an e-fuel containing vanadium-ions, as shown in **Fig. 1**, has been developed. The cell demonstrated performance advancement when compared with other common direct liquid fuel cells which therefore positioned the e-fuel cell as a potential candidate for commercial applications.^{8, 18-20} The cell employs a thermally treated graphite felt

anode, a Pt/C coated carbon paper cathode, and an ion exchange membrane (IEM). As an indispensable component in this system, the IEM is not only needed to provide ion conduction channels for protons, but to also effectively suppress the permeation of reactive species.^{7, 21-23} Hence, the properties of the IEM is of considerable importance in determining the e-fuel cell performance. Up to date, the commercial Nafion series membranes produced by DuPont are the most extensively adopted membrane in fuel cells, by virtue of their superior conductivity and excellent mechanical and chemical stabilities.^{9, 22} Therefore, in this work, to examine the performances of Nafion membranes and identify the membrane suitable for liquid e-fuel cell application, four Nafion membranes with different thicknesses have been studied and characterized at both membrane and cell-level. It is found that the membrane thickness is a crucial factor influencing the cell performance especially due to its critical effects on the membrane area resistance, as well as vanadium-ion crossover rate. Furthermore, it is also found that the cell using the thinnest membrane (Nafion 211) provides the highest peak power density of 363.2 mW cm⁻², while the cell using the thickest membrane (Nafion 117) demonstrates the longest self-discharge duration of 38.2 hours.

2. Experiment

2.1 Fabrication of the e-fuel cell and liquid e-fuel

The membrane electrode assembly (MEA) of 2.0 cm × 2.0 cm was prepared as previously reported.¹⁸ The thermally treated graphite felt was used as the anode, while the cathode used a Pt/C coated carbon paper (~ 0.5 mg cm⁻²). Four Nafion series membranes with different thicknesses including Nafion 117, Nafion 115, Nafion 212, and Nafion 211 were pre-treated following the standard procedures, which in more details involves successively boiling for an

hour in H₂O₂ solution (3 wt. %), deionized (DI) water, 1.0 M sulfuric acid solution, and DI water before further use. The prepared MEA was then assembled into a home-made e-fuel cell fixture, which contains a flow field engraved with serpentine flow channel, current collector, aluminum heating plate, and plastic endplate as reported before.¹⁸ To obtain the e-fuel, VOSO₄ was first dissolved in H₂SO₄, followed by charging the solution using a typical flow cell.

2.2 Membrane-level characterizations

2.2.1 Proton conductivity and area resistance

Before measuring the conductivity and area resistance for each membrane, corresponding samples were immersed in 3.0 M H₂SO₄ solution for 24 hours. Afterwards, a home-made cell was used to conduct the electrochemical impedance spectroscopy (EIS) for the membrane at a frequency range between 100 - 10⁵ Hz using the electrochemical workstation (Autolab PGSTAT 302N, Netherlands). The membrane area resistance (AR) was obtained using the equation:

$$AR = R \times S \quad (1)$$

where R and S is the real-axis intercepts of the Nyquist plots and the effective area of the sample, respectively. In the meanwhile, the membrane conductivity (σ) was calculated by:

$$\sigma = \frac{L}{RS} \quad (2)$$

where L is the membrane thickness.

2.2.2 Vanadium-ion permeability/crossover rates

The vanadium-ion permeability across the membranes was examined using a typical H-cell set-up, where the left reservoir contains 10 ml of e-fuel with 1.0 M V²⁺ ions in 3.0 M H₂SO₄

while the opposite side was filled with 10 ml of 1.0 M MgSO₄ in 3.0 M H₂SO₄ to minimize the osmotic pressure and ensure the balance of ionic strength between the two sides of the H-cell.²⁴ Before testing, the solutions at both sides of the H-cell were purged with N₂ and a layer of paraffin oil was added on the top of the solution to prevent the oxidation of V²⁺ ions by air. The UV-visible spectrophotometer (HALO DB-20) was used to test the vanadium ions concentration in the solution at right side reservoir. Thereafter, the corresponding vanadium ions permeability of each membrane was determined based on the following equation:

$$V_R \frac{dc_R}{dt} = A \frac{P}{L} [c_L - c_R(t)] \quad (3)$$

where V_R stands for the MgSO₄ solution volume, c_L and c_R is the vanadium ions concentration at the left and right-side reservoir, respectively. P is the vanadium ions permeability.

2.3 Cell-level performance characterizations

The polarization and self-discharge tests of the cell were performed by the fuel cell test system (Arbin BT2000, Arbin Instruments). During the polarization test, the e-fuel of 0.5 M V²⁺ ions in 3.0 M H₂SO₄ were fed to the anode, while pure oxygen was provided to the cathode side at 250 sccm. The self-discharge test was conducted with the same cell structure while ambient air was provided at its cathode side. During the self-discharge test, the cell voltage variation was recorded continuously until it drops below 0.6 V. After the self-discharge test, the scanning electron microscope (SEM) images were obtained for all cathodes of the e-fuel cell employing different membranes to observe the morphology changes in the cathodes.

3. Results and discussion

3.1 Membrane characterization

3.1.1 Proton conductivity and area resistance

As discussed, a major requirement for IEM is to allow the ease of charge carriers transport so as to lower ohmic overpotential and further achieve a superior cell performance.²² It is hence an essential requirement for the membrane to possess superior ionic conductivity as well as low area resistance. Here, the ionic conductivities and the area resistances of four Nafion series membranes with different thicknesses were examined as shown in **Fig. 2**. It is shown that, different Nafion membranes exhibit different conductivities and the membrane with thinner thickness is found to possess a lower ionic conductivity, which are consistent with the results reported before.²⁵⁻²⁷ This trend was suggested to be attributed to the extrusion process during the fabrication of the membrane,^{27, 28} where the thinner membranes may be produced at higher pressures, which could lead to the closure of some ion and water transport channels and further reduce the conductivity of the membrane. In contrast, the area resistance, which is another parameter commonly employed to assess the ohmic resistance of membranes, demonstrates a different trend as shown in **Fig. 2**. It is found that the membrane area resistance obviously increases from 0.17 to 0.44 $\Omega \text{ cm}^{-2}$ with the increment of membrane thickness, which in other words indicates that the membrane ohmic loss enlarges with the increment of membrane thickness. In summary, while the thicker Nafion membrane is found to possess a higher ionic conductivity, it also presents a higher area resistances and is therefore considered that the membrane thickness exert a large influence on the cell performance.

3.1.2 Vanadium-ion permeability/crossover rates

In addition to provide ion conduction channels for charge carriers to transport freely across the

membrane, another major function of the membrane is to separate the anode from the cathode and suppress the crossover of reactive species.²² The crossover of e-fuel from anode to cathode would not only lead to the loss of reactive species and thereby lead to severe capacity loss,^{29, 30} but could also induce mixed potential and hence enlarges overpotential loss at the cathode.^{18, 31} To achieve a superior cell performance, the determination of crossover rate and permeability of vanadium ions in the liquid e-fuel through membranes of different thicknesses is thus of vital importance. In this work, a typical H-cell set-up is applied for investigating the membrane permeability through the UV-visible spectroscopy and the obtained results are discussed in the following sections.

3.1.2.1 Determination of molar absorptivity

To enable the accurate calculation of vanadium ions concentration in an arbitrary solution, it is essential to obtain the molar absorptivity coefficients of V^{2+} and V^{3+} ions before conducting the membrane permeability test.^{32, 33} To begin with, the UV-visible spectra for V^{2+} and V^{3+} ions of various concentrations in 3.0 M H_2SO_4 are obtained as shown in **Fig. 3 (a)** and **(d)**, respectively. It is observed that the peak absorbance of V^{2+} ions at 570 nm and 855 nm and the peak absorbance of V^{3+} ions at 400 nm and 610 nm are all consistent with the results previously reported.³² Afterwards, the absorbance at 855 nm is measured to calculate the absorptivity coefficient of V^{2+} ions, while the peak absorbance at 610 nm is chosen to determine V^{3+} ions concentration.³² The relationship between the concentrations of V^{2+} and V^{3+} ions and the peak absorbance are calculated according to the Beer's law as follows:³²

$$A = \epsilon bC = sC \quad (4)$$

where A refers to the absorbance, ϵ represents the molar absorptivity, b is the path length

through the cell which is a constant for the same cuvettes, and C is the concentration. s is the product of ϵb , which in other words is the slope determined from the Beer's law plots as shown in **Fig. 3 (b-c)** and **(e-f)**. It is observed that the obtained peak absorbances at both 610 nm and 855 nm show an excellent linear relationship with the concentrations of V^{2+} and V^{3+} ions.

Considering the inevitable oxidation of V^{2+} to V^{3+} ions during the tests, the following method where the peak absorbance at a certain wavelength is the sum of the individual absorbance of each ion at this wavelength is employed:

$$A_{610\text{ nm}} = s_{v^{2+}}^{610\text{ nm}} C_{v^{2+}} + s_{v^{3+}}^{610\text{ nm}} C_{v^{3+}} \quad (5)$$

$$A_{855\text{ nm}} = s_{v^{2+}}^{855\text{ nm}} C_{v^{2+}} + s_{v^{3+}}^{855\text{ nm}} C_{v^{3+}} \quad (6)$$

By solving these two equations simultaneously, the concentrations of V^{2+} and V^{3+} ions in a mixed solution can therefore be determined, which thereafter can be used to calculate the total vanadium-ion concentration in an arbitrary solution.

3.1.2.2 Crossover rate of vanadium ions

The typical H-cell set-up, as shown in **Fig. 4 (a)**, is employed to examine the vanadium ions crossover rate through each membrane. The left and right reservoir of the H-cell are filled with the e-fuel of 1.0 M V^{2+} ions in 3.0 M H_2SO_4 and 1.0 M $MgSO_4$ in 3.0 M H_2SO_4 , respectively.

The UV-visible spectra are then obtained for the solution in the right reservoir at regular time intervals (every 12 hours) to measure the peak absorbance change at 610 nm and 855 nm.

Afterwards, the total vanadium ions concentrations are calculated as shown in **Fig. 4 (a)**. It is seen that the vanadium ions concentration at the right side of the H-cell increases as time elapses and the H-cell assembled with thinner membrane demonstrates a larger slope of vanadium-ion concentration change. The permeability and crossover rate of each membrane

are then calculated and shown in **Fig. 4 (b)**. The results revealed that, similar to the ionic conductivity results as presented above, thinner Nafion membrane is found to possess a lower vanadium-ion permeability, however, with a higher crossover rate. Such results therefore prove that the membrane with larger thickness can effectively restrict the transport of e-fuel through it and thereby reduce fuel loss especially during long-term operation.³⁴

3.2 Cell performance characterization

3.2.1 Polarization curves

As discussed in the previous sections, membrane thickness plays a pivotal role towards determining the area resistance and crossover rates of reactive species. Hence, to directly investigate the effects of membrane thickness on the cell performance, the polarization curves of the cell using four different membranes are obtained (**Fig. 5 (a)**). The membrane with thinner thickness is found to exhibit a better cell performance including a higher maximum current density and peak power density. In more detail, the cell assembled with the thinnest membrane achieves the highest peak power density of 363.2 mW cm^{-2} , which even outperforms many conventional direct liquid fuel cells.^{16, 35, 36} It is further observed that at the middle current density region, the cell with thinnest membrane demonstrates the slowest decrease of cell voltage, due to low ohmic loss. Such a phenomenon therefore indicates that the membrane area resistance is a crucial parameter towards determining the cell performance. In summary, it is considered that thinner membrane should be adopted when a higher peak power density is the major focus for the e-fuel cell.

3.2.2 Self-discharge behavior

The inevitable crossover of reactive species through the membrane would lead to the loss of fuel and thereby induce self-discharge phenomenon inside the fuel cell.^{18, 37} Hence, to investigate the effects of membrane thickness on the self-discharge behavior at cell-level, experiments are conducted with the cell using four different membranes. The self-discharge curves displayed in **Fig. 5(b)** illustrate that, the open circuit voltage (OCV) of the cell increases gradually with the increment of membrane thickness. Such a phenomenon stems from the fact that the thinner membrane possesses a higher vanadium ions crossover rate, as proved by the permeability test, which therefore results in the presence of more e-fuel at the cathode side and thereby induce a larger potential loss arising from the undesired mixed potential.¹⁸ During the self-discharge test, the OCVs of all the e-fuel cells (each with one of the four membranes) decrease with time and a sudden voltage drop is observed when the e-fuel is exhausted. The test duration is found to decrease from 38.2 h to 7.2 h with the decrease of membrane thickness, which hence demonstrates that the thicker membranes can effectively alleviate net vanadium crossover and thereby lead to a longer test duration. After the self-discharge test, the exhausted e-fuel were kept circulating through the cell for over 100 hours before the cells were disassembled for the purpose of studying the effects of the permeated vanadium ions on the Pt catalysts at the cathode. The SEM images are then obtained for the cathodes assembled with membranes of different thicknesses to examine their morphology changes as shown in **Fig. 6**. It can be seen that, all the cathodes show a much rougher morphology in comparison to the pristine ones, while the cathode assembled with thinnest membrane shows a much more obvious evidence of corrosion. Such a variation thereby proves that the thinner membrane

could lead to a more severe crossover of vanadium ions and further causes a more serious corrosion on the catalyst surface. In summary, it is considered that the membrane with larger thickness is more suitable for long-term operation, where the e-fuel capacity can be better preserved, and the cell can be ensured with better stability. Furthermore, during the real application of this e-fuel cell in the future, DI water should be pumped through the cathode side of the cell after cell operation so as to remove the e-fuel permeated through the membrane and thereby alleviate the degradation of the cell cathode.

4. Summary

In this work, a comparative study has been performed to examine the performances of four Nafion membranes with different thicknesses for application in a liquid e-fuel cell at both membrane-level and cell-level. It is found that the membrane thickness is a crucial parameter for determining membrane area resistance, as well as vanadium crossover rate, which thereby possesses a great impact on the cell performance. In addition, it is also found that the thinner membrane is preferable to achieve a higher peak power density for the cell, due to its lower area resistance, while the membrane with larger thickness is more suitable to meet the requirement for long-term operation, as it can effectively reduce the e-fuel permeation and protect the catalysts at the cathode. Hence, it is believed that by developing membranes with a satisfactory proton conductivity and vanadium ions permeability balance, the liquid e-fuel cell performance can be further boosted.

Acknowledgement

This work was supported by a grant from the National Natural Science Foundation of China (No. 52022003).

References

- 1 Niether, C., Faure, S., Bordet, A., Deseure, J., Chatenet, M., Carrey, J., Chaudret, B. and Rouet, A. (2018). Improved water electrolysis using magnetic heating of FeC–Ni core–shell nanoparticles. *Nature Energy* 3, 476-483.
- 2 Koenigsmann, C. and Wong, S. S. (2011). One-dimensional noble metal electrocatalysts: a promising structural paradigm for direct methanol fuel cells. *Energy Environ. Sci.* 4, 1161-1176.
- 3 Ren, P., Pei, P., Li, Y., Wu, Z., Chen, D. and Huang, S. (2020). Degradation mechanisms of proton exchange membrane fuel cell under typical automotive operating conditions. *Progr. Energy Combust. Sci.* 80, 100859.
- 4 Luo, F., Roy, A., Silvioli, L., Cullen, D. A., Zitolo, A., Sougrati, M. T., Oguz, I. C., Mineva, T., Teschner, D. and Wagner, S. (2020). P-block single-metal-site tin/nitrogen-doped carbon fuel cell cathode catalyst for oxygen reduction reaction. *Nat. Mater.* 19, 1215-1223.
- 5 Zhou, X., Zhao, T., An, L., Wei, L. and Zhang, C. (2015). The use of polybenzimidazole membranes in vanadium redox flow batteries leading to increased coulombic efficiency and cycling performance. *Electrochim. Acta* 153, 492-498.
- 6 Zhou, X., Zhao, T., An, L., Zeng, Y. and Wei, L. (2016). Modeling of ion transport through a porous separator in vanadium redox flow batteries. *J. Power Sources* 327, 67-76.
- 7 Steele, B. C. and Heinzl, A., in *Materials for sustainable energy: a collection of peer-reviewed Research and review articles from nature publishing group*, World Scientific, 2011, pp. 224-231.
- 8 Shi, X., Huo, X., Esan, O. C., An, L. and Zhao, T. (2021). Performance characteristics of a liquid e-fuel cell. *Appl. Energy* 297, 117145.
- 9 Miyake, J., Taki, R., Mochizuki, T., Shimizu, R., Akiyama, R., Uchida, M. and Miyatake, K. (2017). Design of flexible polyphenylene proton-conducting membrane for next-generation fuel cells. *Sci. Adv.* 3, eaao0476.
- 10 Song, Y., Zhang, C., Ling, C.-Y., Han, M., Yong, R.-Y., Sun, D. and Chen, J. (2020). Review on current research of materials, fabrication and application for bipolar plate in proton exchange membrane fuel cell. *Int. J. Hydrogen Energy* 45, 29832-29847.
- 11 Liu, H., Song, C., Zhang, L., Zhang, J., Wang, H. and Wilkinson, D. P. (2006). A review of anode catalysis in the direct methanol fuel cell. *J. Power Sources* 155, 95-110.
- 12 Züttel, A. (2003). Materials for hydrogen storage. *Mater. Today* 6, 24-33.
- 13 Feng, Y., Liu, H. and Yang, J. (2017). A selective electrocatalyst–based direct methanol fuel cell operated at high concentrations of methanol. *Sci. Adv.* 3, e1700580.
- 14 Zhang, Y., Huang, B., Luo, G., Sun, T., Feng, Y., Wang, Y., Ma, Y., Shao, Q., Li, Y. and Zhou, Z. (2020). Atomically deviated Pd-Te nanoplates boost methanol-tolerant fuel cells. *Sci. Adv.* 6, eaba9731.
- 15 Zhao, X., Yin, M., Ma, L., Liang, L., Liu, C., Liao, J., Lu, T. and Xing, W. (2011). Recent advances in catalysts for direct methanol fuel cells. *Energy Environ. Sci.* 4, 2736-2753.
- 16 Martinaiou, I., Videla, A. H. M., Weidler, N., Kuebler, M., Wallace, W. D. Z., Paul, S.,

- Wagner, S., Shahraei, A., Stark, R. W. and Specchia, S. (2020). Activity and degradation study of an Fe-NC catalyst for ORR in Direct Methanol Fuel Cell (DMFC). *Appl. Catal. B* 262, 118217.
- 17 Jiang, H., Wei, L., Fan, X., Xu, J., Shyy, W. and Zhao, T. (2019). A novel energy storage system incorporating electrically rechargeable liquid fuels as the storage medium. *Sci. Bull.* 64, 270-280.
- 18 Shi, X., Huo, X., Ma, Y., Pan, Z. and An, L. (2020). Energizing Fuel Cells with an Electrically Rechargeable Liquid Fuel. *Cell Rep. Phys. Sci.* 1, 100102.
- 19 Shi, X., Dai, Y., Esan, O. C., Huo, X., An, L. and Zhao, T. (2021). A Passive Fuel Cell Fed with an Electrically Rechargeable Liquid Fuel. *ACS Appl. Mater. Interfaces.*
- 20 Shi, X., Huo, X., Esan, O. C., Ma, Y., An, L. and Zhao, T. (2021). A liquid e-fuel cell operating at -20°C . *J. Power Sources* 506, 230198.
- 21 Park, H. B., Kamcev, J., Robeson, L. M., Elimelech, M. and Freeman, B. D. (2017). Maximizing the right stuff: The trade-off between membrane permeability and selectivity. *Science* 356.
- 22 Shi, X., Esan, O. C., Huo, X., Ma, Y., Pan, Z., An, L. and Zhao, T. (2021). Polymer Electrolyte Membranes for Vanadium Redox Flow Batteries: Fundamentals and Applications. *Progr. Energy Combust. Sci.* 85, 100926.
- 23 Zhou, X., Zhao, T., An, L., Zeng, Y. and Zhu, X. (2016). Performance of a vanadium redox flow battery with a VANADion membrane. *Appl. Energy* 180, 353-359.
- 24 Wang, N., Zhang, F., Zhang, R., Zhou, W. and Lu, D. (2019). Sulfonation of Poly (phenylene oxide) Anion Exchange Membrane for All Vanadium Flow Redox Battery. *Int. J. Electrochem. Sci* 14, 5508-5520.
- 25 Tsampas, M., Pikos, A., Brosda, S., Katsaounis, A. and Vayenas, C. (2006). The effect of membrane thickness on the conductivity of Nafion. *Electrochim. Acta* 51, 2743-2755.
- 26 Dimitrova, P., Friedrich, K., Vogt, B. and Stimming, U. (2002). Transport properties of ionomer composite membranes for direct methanol fuel cells. *J. Electroanal. Chem.* 532, 75-83.
- 27 Schafner, K., Becker, M. and Turek, T. (2019). Membrane resistance of different separator materials in a vanadium redox flow battery. *J. Membr. Sci.* 586, 106-114.
- 28 Slade, S., Campbell, S., Ralph, T. and Walsh, F. (2002). Ionic conductivity of an extruded Nafion 1100 EW series of membranes. *J. Electrochem. Soc.* 149, A1556.
- 29 Won, S., Oh, K. and Ju, H. (2015). Numerical analysis of vanadium crossover effects in all-vanadium redox flow batteries. *Electrochim. Acta* 177, 310-320.
- 30 Sun, C., Chen, J., Zhang, H., Han, X. and Luo, Q. (2010). Investigations on transfer of water and vanadium ions across Nafion membrane in an operating vanadium redox flow battery. *J. Power Sources* 195, 890-897.
- 31 Scott, K., Argyropoulos, P. and Sundmacher, K. (1999). A model for the liquid feed direct methanol fuel cell. *J. Electroanal. Chem.* 477, 97-110.
- 32 Choi, N. H., Kwon, S.-k. and Kim, H. (2013). Analysis of the oxidation of the V (II) by dissolved oxygen using UV-visible spectrophotometry in a vanadium redox flow battery. *J. Electrochem. Soc.* 160, A973.
- 33 Brooker, R. P., Bell, C. J., Bonville, L. J., Kunz, H. R. and Fenton, J. M. (2015). Determining vanadium concentrations using the UV-Vis response method. *J.*

- Electrochem. Soc. *162*, A608.
- 34 Jiang, B., Wu, L., Yu, L., Qiu, X. and Xi, J. (2016). A comparative study of Nafion series membranes for vanadium redox flow batteries. *J. Membr. Sci.* *510*, 18-26.
- 35 Souza, F. M., Nandenha, J., Batista, B., Oliveira, V., Pinheiro, V., Parreira, L., Neto, A. and Santos, M. (2018). PdxNby electrocatalysts for DEFC in alkaline medium: stability, selectivity and mechanism for EOR. *Int. J. Hydrogen Energy* *43*, 4505-4516.
- 36 Sun, X., Li, Y. and Li, M.-J. (2019). Highly dispersed palladium nanoparticles on carbon-decorated porous nickel electrode: An effective strategy to boost direct ethanol fuel cell up to 202 mW cm⁻². *ACS Sustain. Chem. Eng.* *7*, 11186-11193.
- 37 Chen, D., Wang, S., Xiao, M. and Meng, Y. (2010). Preparation and properties of sulfonated poly (fluorenyl ether ketone) membrane for vanadium redox flow battery application. *J. Power Sources* *195*, 2089-2095.

Figure captions

Figure 1 Working principle of an e-fuel cell.

Figure 2 Ionic conductivities and area resistances of the Nafion series membranes.

Figure 3 (a) The UV-visible spectra of the e-fuel with various V^{2+} ions concentrations; and Beer's law plot for V^{2+} ions (b) @ 610 nm and (c) @ 855 nm. (d) The UV-visible spectra of the e-fuel with various V^{3+} ions concentrations; and Beer's law plot for V^{3+} ions (e) @ 610 nm and (f) @ 855 nm.

Figure 4 (a) Comparison of the concentration of vanadium ions in the right reservoir of the H-cell using four different membranes. (b) Permeabilities and crossover rates of four membranes.

Figure 5 (a) Polarization curves and power density curves and (b) self-discharge curves of this liquid e-fuel cell with various membranes.

Figure 6 SEM image of (a-b) the pristine cathode; and the cathodes assembled with (c) Nafion 117, (d) Nafion 115, (e) Nafion 212, and (f) Nafion 211.

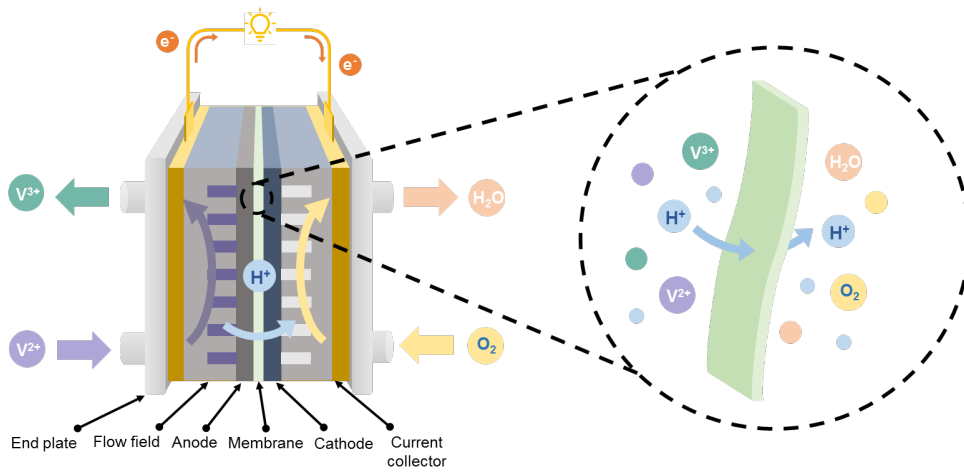


Figure 1 Working principle of an e-fuel cell.

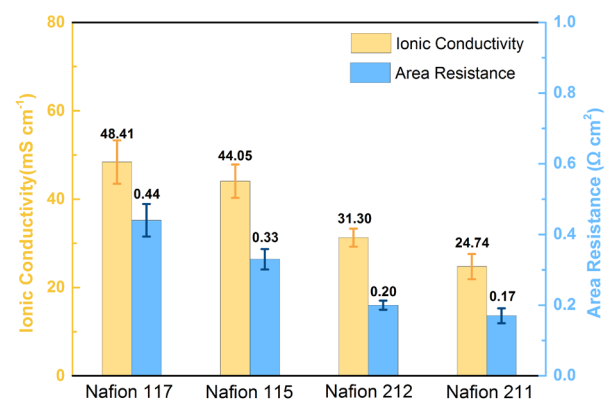


Figure 2 Ionic conductivities and area resistances of the Nafion series membranes.

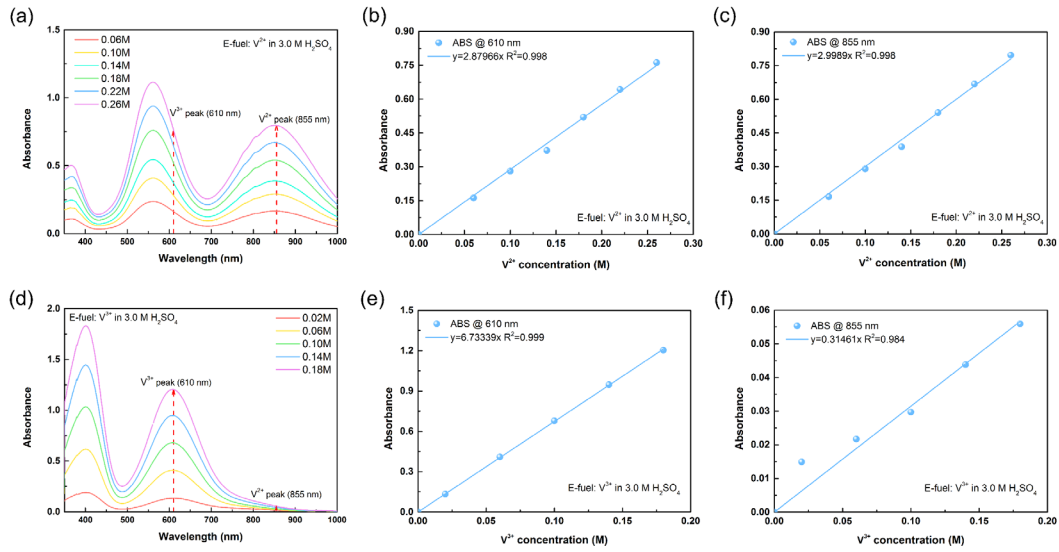


Figure 3 (a) The UV-visible spectra of the e-fuel with various V^{2+} ions concentrations; and Beer's law plot for V^{2+} ions (b) @ 610 nm and (c) @ 855 nm. (d) The UV-visible spectra of the e-fuel with various V^{3+} ions concentrations; and Beer's law plot for V^{3+} ions (e) @ 610 nm and (f) @ 855 nm.

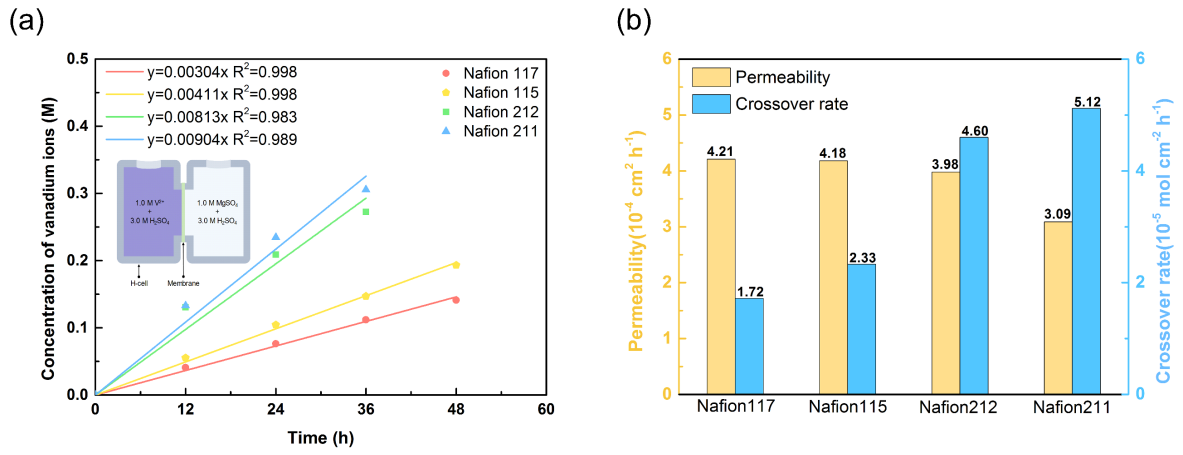


Figure 4 (a) Comparison of the concentration of vanadium ions in the right reservoir of the H-cell using four different membranes. (b) Permeabilities and crossover rates of four membranes.

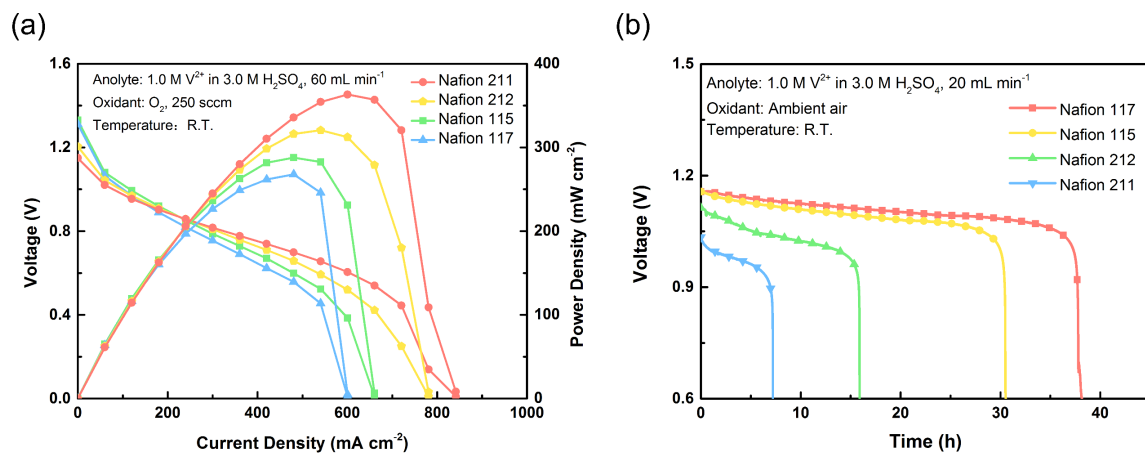


Figure 5 (a) Polarization curves and power density curves and (b) self-discharge curves of this liquid e-fuel cell with various membranes.

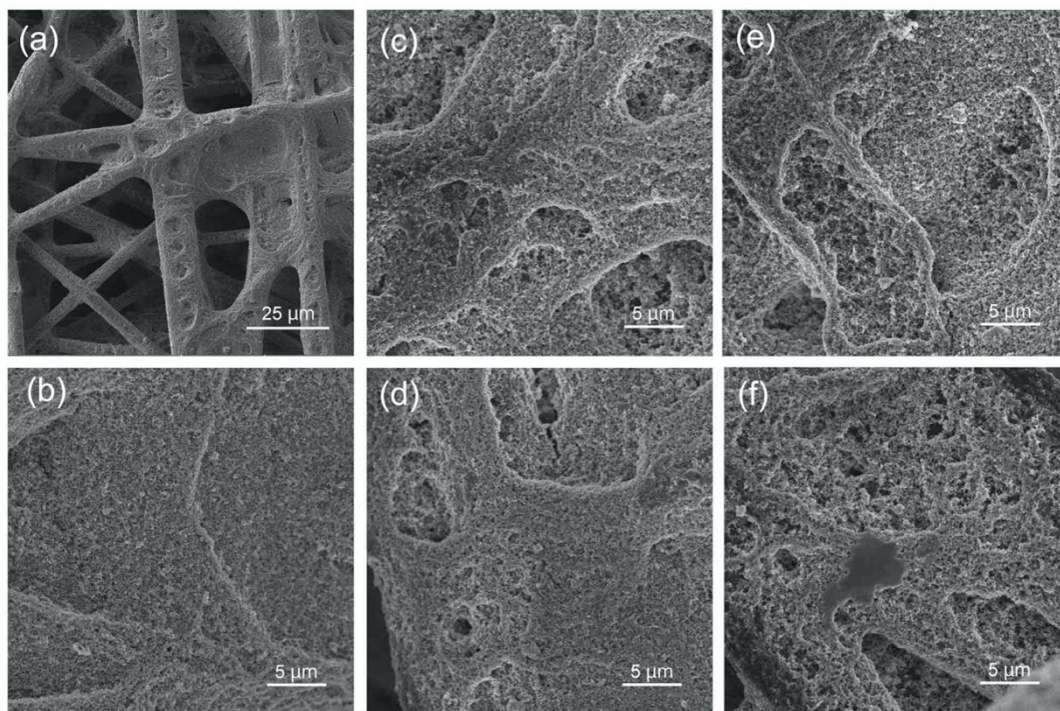


Figure 6 SEM image of (a-b) the pristine cathode; and the cathodes assembled with (c) Nafion 117, (d) Nafion 115, (e) Nafion 212, and (f) Nafion 211.